crystals

MDPI

Article

Pseudo-Polymorphism in 2-Pyridylmethoxy Cone Derivatives of *p-tert*-butylcalix[4]arene and *p-tert*-butylhomooxacalix[n]arenes

Siddharth Joshi [1], Neal Hickey [1], Paula M. Marcos [2,3] and Silvano Geremia [1,*]

[1] Centre of Excellence in Biocrystallography, Department of Chemical and Pharmaceutical Sciences, University of Trieste, Via L. Giorgieri 1, 34127 Trieste, Italy; siddharth.joshi@units.it (S.J.); nhickey@units.it (N.H.)
[2] Centro de Química Estrutural, Institute of Molecular Sciences, Faculdade de Ciências, Universidade de Lisboa, Edifício C8, 1749-016 Lisboa, Portugal; pmmarcos@ciencias.ulisboa.pt
[3] Faculdade de Farmácia, Universidade de Lisboa, Av. Prof. Gama Pinto, 1649-003 Lisboa, Portugal
* Correspondence: sgeremia@units.it

Abstract: This paper investigates pseudo-polymorphism in 2-pyridylmethoxy derivatives of *p-tert*-butylcalix[4]arene (**PyC4**), *p-tert*-butyldihomooxa-calix[4]arenes (**PyHOC4**), and *p-tert*-butylhexahomotrioxacalix[3]arenes (**PyHO3C3**), presenting 11 crystal structures with 15 crystallographically independent molecules. The macrocycle of **PyC4** is smaller and less flexible with respect to those of **PyHOC4** and **PyHO3C3,** and in solution, the cone conformation of these three molecules exhibits different point symmetries: C_4, C_s, and C_3, respectively. A correlation is observed between the macrocycle's structural rigidity and the number of pseudo-polymorphs formed. The more rigid **PyC4** displays a higher number (six) of pseudo-polymorphs compared to **PyHOC4** and **PyHO3C3**, which exhibit a smaller number of crystalline forms (three and two, respectively). The X-ray structures obtained show that the conformation of the macrorings is primarily influenced by the presence of an acetonitrile guest molecule within the cavity, with limited impact from crystal packing and intermolecular co-crystallized solvent molecules. Notably, both calix[4]arene derivatives produce a host–guest complex with acetonitrile, while the most flexible and less aromatic **PyHO3C3** does not give crystals with acetonitrile as the guest. Intertwined 1D and 2D solvent channel networks were observed in the **PyHOC4-hexane** and in the **PyHO3C3-H_2O-MeOH** crystal structures, respectively, while the other pseudopolymorphs of **PyHOC4** and **PyHO3C3** and all **PyC4** crystal forms exhibit closely packed crystal structures without open channels.

Keywords: calixarene; dihomooxacalixarene; hexahomotrioxacalixarene; pseudopolymorphism; X-ray diffraction

Citation: Joshi, S.; Hickey, N.; Marcos, P.M.; Geremia, S. Pseudo-Polymorphism in 2-Pyridylmethoxy Cone Derivatives of *p-tert*-butylcalix[4]arene and *p-tert*-butylhomooxacalix[n]arenes. *Crystals* **2024**, *14*, 343. https://doi.org/10.3390/cryst14040343

Academic Editor: Waldemar Maniukiewicz

Received: 13 March 2024
Revised: 30 March 2024
Accepted: 1 April 2024
Published: 3 April 2024

1. Introduction

In the last three decades, the field of calixarenes-based host–guest chemistry has garnered significant scientific interest due to its diverse applications in the domain of supramolecular chemistry, including sensor chemistry, catalysis, and drug delivery [1–17]. Research efforts have particularly focused on the interaction between calixarenes, especially those with oxygen donor atoms on the lower rim, and metal cations, predominantly alkali and alkaline earths [4,18,19]. Moreover, calixarenes functionalized with both N-donor and O-donor atoms have been investigated for their effectiveness in complexing transition metals [16,20], heavy metals [16,21], and lanthanide cations [18,22]. Further enhancements to calixarene properties have been explored through modifications involving the incorporation of 2-pyridyl-methyl pendant groups on the lower rim. This exploration has resulted in the synthesis of *p-tert*-butyl-*tetrakis*(2-pyridylmethyl)oxycalix[4]arene (**PyC4**) [23] (Figure 1). The cone conformation of this calixarene shows complexation properties towards Na^+ [24], Ag^+ [25], and lantanide ions [26].

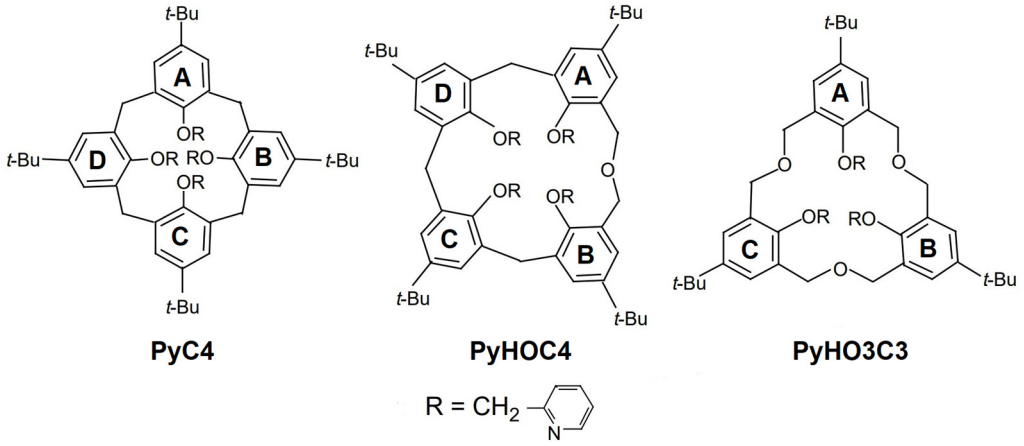

Figure 1. Chemical structures of the three macrocycles.

Additionally, homooxacalixarenes [27], calixarene analogs in which one or more CH_2 bridges are replaced by CH_2OCH_2 groups, were investigated. Notable among these derivatives, dihomooxacalix[4]arene with one CH_2OCH_2 bridge (**PyHOC4**) and hexahomotrioxacalix[3]arene with three CH_2OCH_2 bridges (**PyHO3C3**) (Figure 1) are attracting attention for their higher conformational flexibility compared to calix[4]arene analogs [26,28,29]. In fact, the comparison shows that the **C4** macrocycle is a 16-membered ring (8 aromatic and 8 single bonds), the **HOC4** macrocycle is an 18-membered ring (8 aromatic and 10 single bonds), and the **HO3C3** macrocycle is also an 18-membered ring which includes more single bonds (6 aromatic and 12 single bonds). However, despite possessing slightly larger cavity sizes than calix[4]arenes, both **HOC4** and **HO3C3** can assume blocked cone conformations when functionalized with bulky groups on the lower rim, such as in **PyHOC4** and in **PyHO3C3**. Furthermore, in the cone conformation, these three molecules exhibit different point symmetries of the macrocycle: **PyC4** has C_4 symmetry, **PyHOC4** has C_s symmetry, while **PyHO3C3** has C_3 symmetry (as shown in Figure 1). It should be noted that these macrorings exhibit significant conformational diversity. Four basic conformations are possible in the case of calix[4]arene: cone, partial cone, 1,2-alternate, and 1,3-alternate [30]. In the case of the dihomooxacalix[4]arene, the situation is more complicated, with ten different stereoisomers: cone, 1,2-alternate, and the enantiomeric pairs of partial-cone-1, partial-cone-3, 1,3-alternate, and 1,4-alternate [31]. For the hexahomotrioxacalix[3]arene, the situation is more simple as only two conformations are possible: cone and partial cone [32]. If the conformation is not blocked by a bulky substituent on the lower rim, the conformations are in equilibrium and interesting examples of crystals with the coexistence of more than one conformer have been reported [33,34]. In previous studies of one of the coauthors, theoretical and solution investigations on the complexation of lanthanide ions by these three macrocycles were reported [26]. In order to further investigate the conformational and binding properties of these macrocycles, we conducted a systematic structural study by single crystal X-ray diffraction on crystals obtained under various crystallization conditions for all three calixarenes in the presence of lanthanide ions. Unfortunately, despite our efforts, none of the crystallization trials produced crystals containing the rare earth Ion complexes. However, during this study, we obtained six pseudo-polymorphs of **PyC4**, three pseudo-polymorphs of **PyHOC4**, and two pseudo-polymorphs of **PyHO3C3**, using analogous crystallization conditions for all three. The pseudo-polymorphs in this study differ in the identity and content of co-crystallized solvent molecules. In the present paper, we describe and compare the accurate crystal structures of these macrocycles obtained using state-of-the-art X-ray diffraction, employing cryo-techniques and synchrotron radiation.

2. Experimental

The calixarenes studied in this work were synthesized according to the literature: **PyC4** [23], **PyHOC4** [35], and **PyHO3C3** [36]. Following a general synthetic route, the cor-

responding parent calixarene was treated with five equivalent of 2-(chloromethyl)pyridine and NaH in dry DMF, under heating and stirring for an extended period of time (from 24 h to 3 days, depending on the calixarene). The products obtained were purified by flash chromatography and/or re-crystallization.

As a general procedure, single crystals of calixarenes were obtained through the slow evaporation of solvents. Near-saturated solutions of the macrocycles were prepared in suitable solvents. The vials, covered with perforated caps, were placed in a crystallization room at 18 °C to evaporate. The rate of evaporation is an experimental variable that depends, to some extent, on the volatility of the solvent. Crystals can grow within hours to days by selecting an appropriate solvent or mixture of solvents, depending on the boiling point, temperature, and, consequently, the evaporation rate. For all three calixarenes, the following solvents or mixtures thereof were used: MeOH, $CHCl_3$, Hexane, DMSO, THF, MeCN, and Toluene. The trials which have produced suitable crystals for X-ray diffraction investigation are reported in Table S1.

The single crystal X-ray diffraction data collection was conducted at the XRD1 beamline of the Elettra synchrotron in Trieste, Italy. The rotating-crystal method was employed, utilizing a Dectris Pilatus 2M area detector and monochromatic radiation with a wavelength of 0.700 Å. Single crystals from the mother liquor were dipped in paratone cryoprotectant, mounted on a nylon loop and flash-frozen under a nitrogen stream at 100 K. Diffraction data were indexed and integrated using the XDS package version 20230630 [37], while scaling was carried out with XSCALE [38]. Structures were solved using the SHELXT 2018/2 program [39] and the refinement was performed with SHELXL 2018/3 [40] by the full-matrix least-squares (FMLS) method on F^2.

For the refinement, non-hydrogen atoms were anisotropically refined with the exception of some disordered groups having a low occupancy factor, which were refined isotropically. The coordinates of the hydrogen atoms of water molecules were freely refined, while for the methyl and hydroxyl groups, only the torsion angles were refined. The other hydrogen atoms, located on the difference Fourier maps, were added at the calculated positions and refined using the riding model. The occupancy factors of the disordered atoms were initially refined and after a few cycles were fixed on the basis of these refinements and on the evaluation of their thermal motions.

Crystal data for **PyC4-MeOH-α**: $C_{68}H_{76}O_4N_4 \cdot 0.2CH_3OH$ (M = 1019.73 g/mol), monoclinic, space group $P2_1/c$ (no. 14), a = 12.004(4) Å, b = 12.090(8) Å, c = 40.691(5) Å, β = 95.857(13) °, V = 5875(2) Å^3, Z = 4, μ = 0.068 mm^{-1}, Dcalc = 1.153 g/cm^3, 92,155 reflections measured ($2.0° \leq 2\Theta \leq 59.2°$), 16,083 unique (Rint = 0.0292, Rsigma = 0.0475) which were used in all calculations. The final R1 was 0.0616 ($I > 2\sigma(I)$) and wR2 was 0.1664 (all data).

Crystal data for **PyC4-H$_2$O-α**: $C_{68}H_{76}O_4N_4 \cdot 0.4H_2O$ (M = 1020.53 g/mol), monoclinic, space group $P2_1/c$ (no. 14), a = 12.005(5) Å, b = 12.121(1) Å, c = 40.565(2) Å, β = 95.98(2) °, V = 5871(2) Å^3, Z = 4, μ = 0.069 mm^{-1}, Dcalc = 1.155 g/cm^3, 108,841 reflections measured ($3.4° \leq 2\Theta \leq 59.2°$), 15,795 unique (Rint = 0.0232, Rsigma = 0.0424) which were used in all calculations. The final R1 was 0.0444 ($I > 2\sigma(I)$) and wR2 was 0.1238 (all data).

Crystal data for **PyC4-MeOH-β**: $C_{68}H_{76}O_4N_4 \cdot 0.75CH_3OH$ (M = 1037.35 g/mol), triclinic, space group P-1 (no. 2), a = 10.410(4) Å, b = 23.014(9) Å, c = 24.874(10) Å, α = 95.813(8) °, β = 90.17(3) °, γ = 97.56(3) °, V = 5876(4) Å^3, Z = 4, μ = 0.070 mm^{-1}, Dcalc = 1.173 g/cm^3, 26,719 reflections measured ($2.2° \leq 2\Theta \leq 43.2°$), 14,199 unique (Rint = 0.0920) which were used in all calculations. The final R1 was 0.0966 ($I > 2\sigma(I)$) and wR2 was 0.2930 (all data).

Crystal data for **PyC4⊂MeCN-MeOH**: $C_{68}H_{76}O_4N_4 \cdot CH_3CN \cdot CH_3OH$ (M = 1086.42 g/mol), monoclinic, space group $P2_1$ (no. 4), a = 13.936(2) Å, b = 15.260(1) Å, c = 14.125(2) Å, β = 92.794(19) °, V = 3000.3(6) Å^3, Z = 2, μ = 0.072 mm^{-1}, Dcalc = 1.203 g/cm^3, 53,801 reflections measured ($2.8° \leq 2\Theta \leq 59.2°$), 16,697 unique (Rint = 0.0392, Rsigma = 0.0418) which were used in all calculations. The final R1 was 0.0407 ($I > 2\sigma(I)$) and wR2 was 0.1131 (all data).

Crystal data for **PyC4⊂MeCN-H$_2$O**: $C_{68}H_{76}O_4N_4 \cdot CH_3CN \cdot 0.2H_2O$ (M = 1057.98 g/mol), triclinic, space group P-1 (no. 2), a = 13.239(2) Å, b = 14.358(1) Å, c = 18.297(2) Å, α = 95.419(8) °,

β = 100.656(11) °, γ = 117.079(9) °, V = 2979.3(6) Å^3, Z = 2, μ = 0.070 mm^{-1}, Dcalc = 1.179 g/cm^3, 56,137 reflections measured (2.2° ≤ 2Θ ≤ 59.2°), 15,954 unique (Rint = 0.0197, Rsigma = 0.0233) which were used in all calculations. The final R1 was 0.0479 (I > 2σ(I)) and wR2 was 0.1333 (all data).

Crystal data for **PyC4**: $C_{68}H_{76}O_4N_4$ (M = 1013.32 g/mol), monoclinic, space group $P2_1/n$ (no. 14), *a* = 15.167(1) Å, *b* = 19.994(6) Å, *c* = 20.267(6) Å, β = 108.878(12) °, V = 5815(4) Å^3, Z = 4, μ = 0.068 mm^{-1}, Dcalc = 1.157 g/cm^3, 106,301 reflections measured (3.0° ≤ 2Θ ≤ 59.2°), 16,910 unique (Rint = 0.0271, Rsigma = 0.0466) which were used in all calculations. The final R1 was 0.0585 (I > 2σ(I)) and wR2 was 0.1666 (all data).

Crystal data for **PyHOC4-DMSO**: $C_{69}H_{78}O_5N_4 \cdot 0.8625C_2H_6SO$ (M = 1109.22 g/mol), triclinic, space group P-1 (no. 2), *a* = 20.98(2) Å, *b* = 22.476(18) Å, *c* = 28.52(3) Å, α = 72.25(2) °, β = 81.425(15) °, γ = 89.765(16) °, V = 12655(22) Å^3, Z = 8, μ = 0.098 mm^{-1}, Dcalc = 1.164 g/cm^3, 101611 reflections measured (2.0° ≤ 2Θ ≤ 43.2°), 29067 unique (Rint = 0.0838, Rsigma = 0.0985) which were used in all calculations. The final R1 was 0.1659 (I > 2σ(I)) and wR2 was 0.5018 (all data).

Crystal data for **PyHOC4⊂MeCN-MeOH**: $C_{69}H_{78}O_5N_4 \cdot CH_3CN \cdot 0.8CH_3OH$ (M = 1110.04 g/mol), triclinic, space group P-1 (no. 2), *a* = 13.969(11) Å, *b* = 14.823(8) Å, *c* = 15.292(5) Å, α = 84.06(3) °, β = 83.01(4) °, γ = 87.134(16) °, V = 3124(3) Å^3, Z = 2, μ = 0.071 mm^{-1}, Dcalc = 1.180 g/cm^3, 20,567 reflections measured (2.6° ≤ 2Θ ≤ 41.0°), 6399 unique (Rint = 0.0543, Rsigma = 0.0605) which were used in all calculations. The final R1 was 0.1326 (I > 2σ(I)) and wR2 was 0.4251 (all data).

Crystal data for **PyHOC4-Hexane**: $C_{69}H_{78}O_5N_4 \cdot 1.5C_6H_{14}$ (M = 1172.61 g/mol), triclinic, space group P-1 (no. 2), *a* = 11.686(5) Å, *b* = 16.604(2) Å, *c* = 17.957(3) Å, α = 88.990(3) °, β = 86.252(5) °, γ = 77.253(5) °, V = 3391(2) Å^3, Z = 2, μ = 0.068 mm^{-1}, Dcalc = 1.148 g/cm^3, 123,862 reflections measured (2.2° ≤ 2Θ ≤ 59.6°), 19,724 unique (Rint = 0.0260, Rsigma = 0.0448) which were used in all calculations. The final R1 was 0.0643 (I > 2σ(I)) and wR2 was 0.1891 (all data).

Crystal data for **PyHO3C3**: $C_{54}H_{63}O_6N_3$ (M = 850.07 g/mol), monoclinic, space group $P2_1/c$ (no. 14), *a* = 24.022(3) Å, *b* = 10.7210(14) Å, *c* = 19.415(5) Å, β = 111.667(7) °, V = 4647(1) Å^3, Z = 4, μ = 0.075 mm^{-1}, Dcalc = 1.215 g/cm^3, 85,480 reflections measured (1.8° ≤ 2Θ ≤ 59.2°), 13,548 unique (Rint = 0.0359, Rsigma = 0.0585) which were used in all calculations. The final R1 was 0.0883 (I > 2σ(I)) and wR2 was 0.2571 (all data).

Crystal data for **PyHO3C3-H_2O-MeOH**: $C_{54}H_{63}O_6N_3 \cdot 4H_2O \cdot CH_3OH$ (M = 954.18 g/mol), monoclinic, space group $P2_1/c$ (no. 14), *a* = 19.430(19) Å, *b* = 14.376(3) Å, *c* = 19.605(8) Å, β = 106.84(5) °, V = 5241(6) Å^3, Z = 4, μ = 0.080 mm^{-1}, Dcalc = 1.209 g/cm^3, 96,321 reflections measured (2.1° ≤ 2Θ ≤ 59.2°), 15,397 unique (Rint = 0.0421, Rsigma = 0.0710) which were used in all calculations. The final R1 was 0.0567 (I > 2σ(I)) and wR2 was 0.1605 (all data).

3. Results and Discussion

3.1. *PyC4*—*Calix[4]arene*

Three different crystal structures of **PyC4** have already been reported in the literature. The first structure was documented by Pappalardo et al. [23]. The diffraction data of this monoclinic crystal form, obtained from a methanol solution, were collected at 21 °C. The structure reveals a co-crystallized solvent molecule with 0.6 occupancy, hydrogen-bonded to a pyridyl N atom orientated away from the cavity of the calixarene, which assumes a pinched cone conformation [23]. The other two crystal structures are two distinct tetragonal forms (P4cc and P4/n space groups) of **PyC4** complexes with Na^+ [24] and Ag^+ [25] ions, respectively, both reported by Danil de Namor et al. In these structures, the calixarene is situated on a fourfold symmetry axis, with the hydrophobic cavity hosting an acetonitrile molecule. At the lower rim, the hydrophilic cavity encapsulates the Ag^+ and Na^+ ions through the ether oxygen and pyridyl nitrogen atoms. A distorted Archimedean square antiprism coordination of the cations is observed for both complexes. The role of metal ion complexation on the lower rim in the preorganization of the calix cup, thereby allowing the complexation of an acetonitrile guest in calix[4]arene-tetrol derivatives, has been

recently reported. This results in the formation of crystals with molecular cavities. On the other hand, different solvents, such as acetonitrile or water, can be used to design Supramolecular Organic Frameworks (SOF) with large hydrophobic or hydrophilic channels, respectively [41]. The different solubility of **PyC4** in various solvents [24] plays an important role in the crystallization process and in the formation of different polymorphs or pseudo-polymorphic solvate crystals containing different co-crystallized solvent molecules.

A summary of the successful crystallization conditions used in the various trials conducted is shown in Table S1. The asymmetric units of the six pseudo-polymorphic structures of **PyC4**, including the co-crystallized solvent molecules, are shown in Figure 2. The crystal data and the structure refinements of the six pseudo-polymorphs, four monoclinic and two triclinic, of **PyC4** are summarized in Table S2.

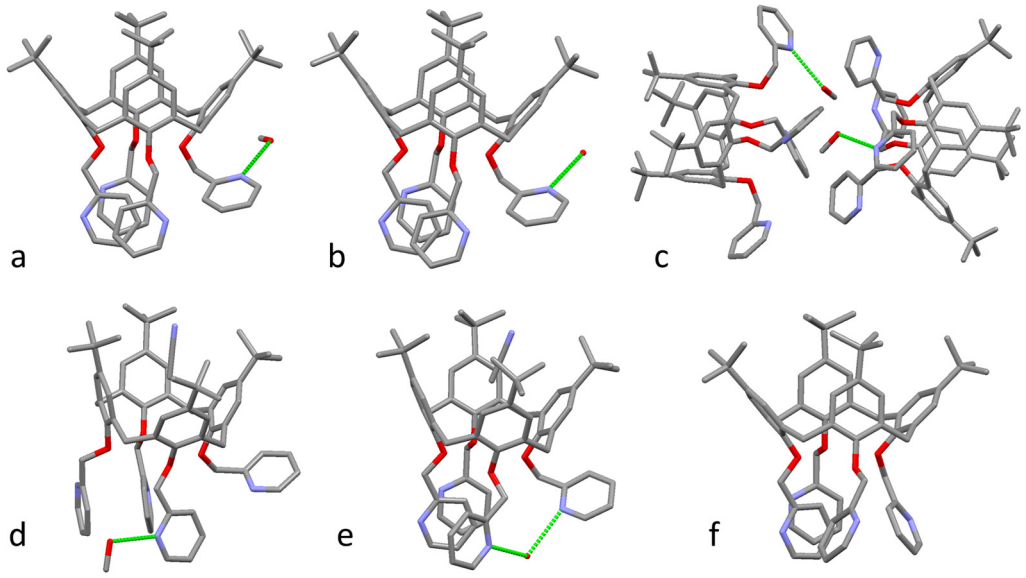

Figure 2. Six asymmetric units of various **PyC4** structures obtained in different solvents: (**a**) **PyC4-MeOH-α**; (**b**) **PyC4-H$_2$O-α**; (**c**) **PyC4-MeOH-β**; (**d**) **PyC4⊂MeCN-MeOH**; (**e**) **PyC4⊂MeCN-H$_2$O;** and (**f**) **PyC4**. H-bonds between calixarene and co-crystallized solvent molecules are represented by green dashed lines. Hydrogen atoms have been omitted and only one position of the disorder groups is shown for better clarity. Atoms are in CPK colors.

The asymmetric unit of the monoclinic crystals of **PyC4-MeOH-α** consist of one molecule of calixarene and co-crystallized methanol molecules disordered in two positions, each with 0.1 occupancy. The solvent molecules are involved in H-bonds with a pyridyl N-acceptor of the arm oriented away from the cavity of the calixarene (Figure 2a). The other three pyridyl groups are almost parallel and stack together (Figure 2a). This structure is analogous to the structure previously reported from room temperature data collection [23]. The high quality of diffraction data collected at a low temperature has permitted us to observe a disorder in the outward oriented pyridyl group involved in the H-bond with the methanol molecule with partial occupancy. The presence in the Fourier difference maps of electron density attributable to the half hydrogen atoms attached to both *orto* positions (with respect to the methylene group) and the thermal factors of the corresponding N/C atoms indicate two overlapped orientations of the pyridyl group rotated by 180°. A second difference in comparison with the published structure is related to the disorder of the co-crystallized methanol molecules and their slight difference in orientation. The D-A H-bond distances are 2.97 and 2.92 Å for our low temperature structure, and 2.81 Å for the room temperature structure. The expected and observed decrease in the cell volume at a low temperature (3.8%) is largely due to the decrease in the b axis (3.6%).

The second crystal of **PyC4** is an isomorphic solvate of **PyC4-MeOH-α**, which differs only in the nature of the co-crystallized solvent molecules (Figure 2b). In this **PyC4-H$_2$O-α**

structure, the methanol site is occupied by a water molecule, split in two positions with an occupancy of 0.1 and 0.3. The origin of the water molecules can be attributed to the hydrate salt used in the crystallization trials (see Supplementary Materials). These co-crystallized water molecules form H-bonds with the nitrogen atoms of the outward orientated pyridyl rings (D-A distances of 2.96 and 2.86 Å, Figure 2b). The pinched cone conformation and the disorder of the pyridyl arm (0.5/0.5) are very similar to those observed in **PyC4-MeOH-α.**

The third structure, **PyC4-MeOH-β**, was obtained from a triclinic non-merohedral twin crystal and corresponds to a second crystal form of **PyC4-MeOH**. The asymmetric unit contains two calix[4]arene molecules, each of which forms an H-bond with co-crystallized MeOH molecules (Figure 2c). These two crystallographic independent solvent molecules have occupancy factors of 0.7 and 0.8, with H-bond D-A distances of 2.97 and 2.85 Å, respectively. The two **PyC4** molecules exhibit very similar conformations, with regard to both the pinched calix[4]arene cones and the orientation of the pyridyl arms (see Supplementary Materials and Figure 2c). All four pyridyl arms are outwards oriented and related by the pseudo-twofold axis of the calix[4]arene, which is a very different conformation with respect to the aromatic stack organization of the three pyridyl moieties observed in the α form. In the β form, the arms attached to the pinched aromatic rings, one of which is involved in the H-bond interaction with the methanol molecule (Figure 3c), are further away from the central axis with respect to the other two pyridyl groups.

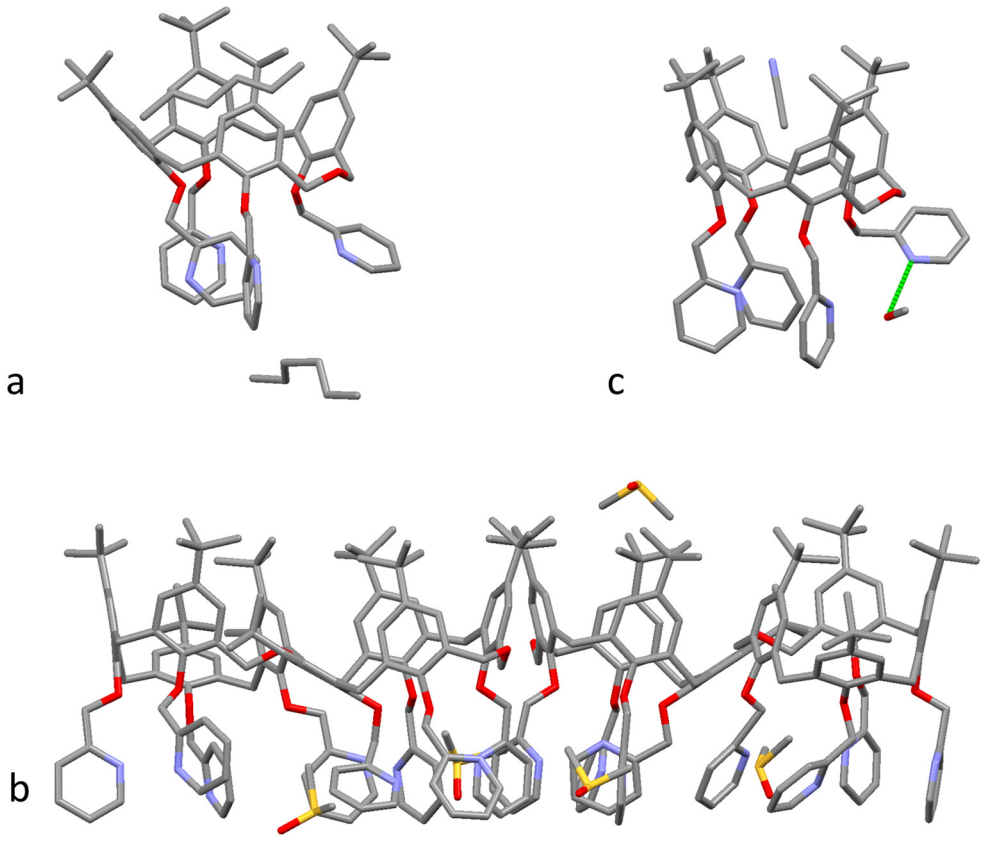

Figure 3. Asymmetric units of three different **PyHOC4** structures obtained in different solvents: (**a**) **PyHOC4-Hexane**; (**b**) **PyHOC4-DMSO;** and (**c**) **PyHOC4⊂MeCN-MeOH**. Hydrogen atoms have been omitted and only one position of the disorder groups is shown for better clarity. Atoms are in CPK colors.

The crystals obtained in the presence of acetonitrile are characterized by the formation of the host–guest complex between **PyC4** and MeCN (**PyC4⊂MeCN**), with the solvent molecule hosted in the calix[4]arene cup. Due to the presence of the guest, which forms the standard C–H···π interactions with the aromatic walls of **PyC4**, the calix[4]arene macrocycle

assumes a more regular cone conformation in the solid state with respect to that observed in the absence of a guest molecule. Two pseudo-polymorphic structures of the **PyC4⊂MeCN** complex were obtained, a monoclinic form with co-crystallized methanol solvent molecules, **PyC4⊂MeCN-MeOH** (Figure 2d), and a hydrated triclinic form, **PyC4⊂MeCN-H_2O** (Figure 2e). In the hydrated triclinic form, the conformation of the pyridyl arms is similar to that found for the α form (Figure 2a,b) with the aromatic stacking of three pyridyl groups, despite the differences in the cone pseudo-symmetry. However, in contrast to the situation observed in the α form, in the **PyC4⊂MeCN-H_2O** structure, the N-atom of the fourth pyridyl, forming the H-bond with the co-crystallized water molecule, points towards the center of the calix[4]arene. The water molecule, with an occupancy factor of 0.2, is hosted more internally, and completes a H-bond bridge with one of the stacked pyridyls, the position of which is slightly adjusted to accommodate the H_2O molecule (Figure 2e). The monoclinic form, **PyC4⊂MeCN-MeOH**, shows a different disposition of the pyridyl arms. One pyridyl involved in a H-bond with a methanol molecule, which shows a two-position disorder of the methyl group (0.8 and 0.2 occupancy factors), is almost parallel to the attached aromatic ring. The opposite pyridyl is almost orthogonal to its attached aromatic ring and stacks with an adjacent pyridyl, while the fourth one is outward oriented (Figure 2d). The comparison with the α and β forms evidences that the two stacked pyridyl arms in the β form are rotated by about 90° with respect to their orientations in the α form, whereas the orientations of the planes of the pyridyl groups involved in H-bond interaction do not change significantly (Figure 2d). This **PyC4⊂MeCN-MeOH** crystal form is the only structure characterized by a non-centrosymmetric polar space group ($P2_1$).

The sixth structure of **PyC4** was obtained from an unsolvated crystal. This structure is characterized by a pinched cone conformation of the cup, with interior dihedral angles between the aromatic rings slightly more closed than in the other pseudo-polymorphs (Table 1). The conformation of the pyridyl arms is characterized by the parallel π-stacking of two aromatic rings, with one orthogonal oriented to these planes. The fourth pyridyl arm is less outwardly oriented in comparison to the solvated structures (Figure 2f).

Table 1. Interior dihedral angles between the aryl–aryl planes observed in the crystal structures. See Figure 1 for the labeling scheme of the arene moieties.

Crystal	A-B	B-C	C-D	D-A
PyC4-MeOH-α	96	94	92	91
PyC4-H_2O-α	96	94	92	91
PyC4-MeOH-β	96	92	94	93
*	96	93	95	93
PyC4⊂MeCN-MeOH	100	102	95	100
PyC4⊂MeCN-H_2O	99	100	97	101
PyC4	86	87	92	93
PyHOC4-DMSO	59	90	103	97
*	58	95	97	98
*	62	91	102	95
*	56	91	99	102
PyHOC4⊂MeCN-MeOH	69	112	105	96
PyHOC4-Hexane	61	77	101	113
			C-A	
PyHO3C3	48	102	36	
PyHO3C3-H_2O-MeOH	62	98	31	

* Dihedral angles of other crystallographic independent molecules.

3.2. ***PyHOC4***—*Dihomooxacalix[4]arene*

Three pseudo-polymorphic structures of dihomooxacalix[4]arene were obtained (Table S3). The first one corresponds to a triclinic crystal with one molecule of **PyHOC4** and 1.5 molecules of *n*-hexane in the asymmetric unit (Figure 3a). The two independent solvent molecules are located in the interstitial spaces between symmetry-related **PyHOC4** molecules. One of these assumes an extended zig-zag conformation and it lies on an inversion center. The cone conformation of the cup is similar to that previously observed for other dihomooxacalix[4]arene derivatives with four substituents on the lower rim, without a guest [42]. The presence of the oxa bridge results in the loss of the pseudo-C2 symmetry of the macrocycle. One of the two planes of the phenyl rings connected to the dihomooxa bridge is oriented outwards from the calixarene cone, while the other is inward oriented, both by about 22° (Table 2). The phenyl ring opposite to the outwards oriented ring is even more outwards oriented (about 47°), while the fourth phenyl ring is almost parallel to the inward oriented phenyl group and therefore it is outwards oriented (Table 2). Despite the differences in the cone conformation, the organization observed for the four pyridyl groups (Figure 3a) is analogous to the one observed for the **PyC4** structure without H-bond interactions (Figure 2f). The crystal packing analysis shows that the hexane solvent molecules are present in an unusual intertwined 1D channel network developed along the crystallographic *a* axis (Figure 4). These channels account for over 20% of the total crystal volume (Table S5).

Table 2. Dihedral canting angles between the aryl planes and the mean planes of the bridging methylene carbon atoms for various calixarenes. Dihedral angles greater than 90° correspond to outward orientations of the plane with respect to the cup. See Figure 1 for the labeling scheme of the arene moieties.

Crystal	A	B	C	D
PyC4-MeOH-α	128	98	128	91
PyC4-H_2O-α	128	98	128	91
PyC4-MeOH-β	136	96	130	89
*	135	93	131	91
PyC4⊂MeCN-MeOH	118	112	117	108
PyC4⊂MeCN-H_2O	121	110	118	109
PyC4	135	85	130	87
PyHOC4-DMSO	117	72	135	102
*	119	76	136	98
*	116	74	134	100
*	119	70	136	103
PyHOC4⊂MeCN-MeOH	105	97	128	112
PyHOC4-Hexane	112	68	137	106
PyHO3C3	57	119	134	
PyHO3C3-H_2O-MeOH	66	110	133	

* Dihedral angles of other crystallographic independent molecules.

A second pseudo-polymorph was obtained in the presence of DMSO solvent. This triclinic form has a large asymmetric unit composed of four **PyHOC4** molecules and 3.45 DMSO molecules distributed over six sites. The cone conformation of all four crystallographic independent molecules is similar to that observed for **PyHOC4-hexane** (Table 2). On the other hand, a high degree of variability is observed for the orientations of the pyridyl groups across the four independent molecules. This variability is also evidenced by the observation of a two-position disorder for three entire pyridyl groups. Two of the independent molecules exhibit an interesting edge–face–edge stacking of three pyridyl

moieties, with the central pyridyl group located at the center of the calixarene on the molecular axis (Figure 3b).

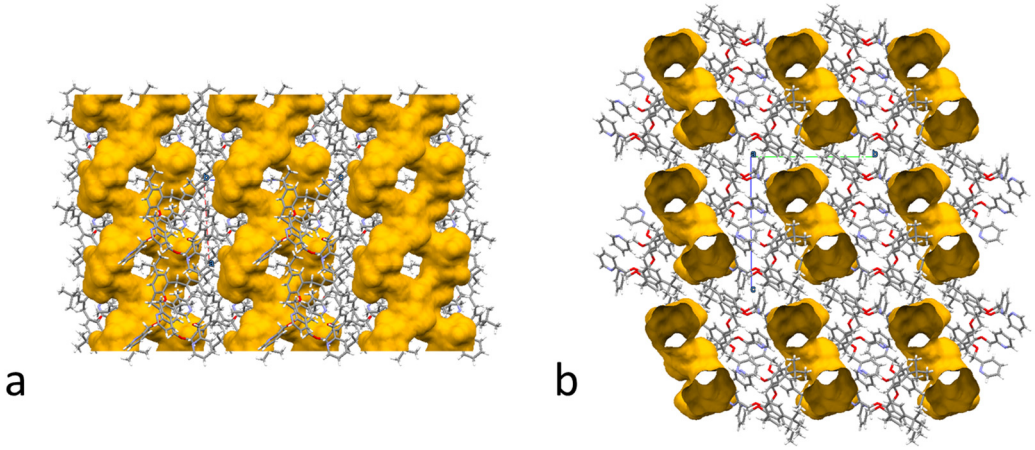

Figure 4. Crystal packing of **PyHOC4-hexane** (**a**) viewed along the crystallographic *b* axis and (**b**) viewed along the crystallographic *a* axis. The surface of the solvent accessible volume calculated with a 1.2 Å probe evidences the intertwined 1D channel network developed along the crystallographic *a* axis. Atoms in CPK colors.

A third crystalline form was obtained in the presence of acetonitrile and methanol. The asymmetric unit contains one host–guest complex between **PyHOC4** and the acetonitrile molecule (**PyHOC4⊂MeCN**) and a methanol molecule H-bonded to an N-atom of a pyridyl arm. As observed in the **PyC4** host–guest complexes described above and in analog dihomooxacalix[4]arenes [42], in the presence of the acetonitrile guest, which forms C–H···π interactions with the aromatic walls of **PyHOC4**, the macrocycle assumes a more open cone conformation (Figure 3c) with respect to that observed in the absence of a guest molecule (Figure 3a,b). In this case, the inward oriented phenyl group is pushed externally and all four aromatic rings show an outwards orientation (Table 2). The methanol molecule found in the crystal structure forms a H-bond with a D-A distance of 2.89 Å. With the exception of the pyridyl involved in the H-bond, which shows a conformation similar to that found in all other pyridyl groups involved in the H-bonds of the **PyC4** structures, the other three pyridyl groups of **PyHOC4⊂MeCN-MeOH** exhibit a two-position disorder (0.5/0.5, 0.5/0.5, and 0.65/0.35 occupancy factors).

3.3. ***PyHO3C3***—*Hexahomotrioxacalix[3]arene*

Two monoclinic crystal forms were characterized for **PyHO3C3**, one anhydrous and one highly hydrated crystal form (Table S4). In the anhydrous form, a single crystallographically independent molecule of **PyHO3C3** is present (Figure 5a), while in the hydrate form, the asymmetric unit contains one **PyHO3C3** molecule, four co-crystallized water molecules, and one co-crystallized methanol molecule, all with full occupancy (Figure 5b). As described above, the thrice-repeated CH_2–O–CH_2 bridge confers higher flexibility to the **PyHO3C3** macrocycle with respect to **PyC4** and **PyHOC4**. The cone conformation of **PyHO3C3** is significantly different in the two crystal forms. Both forms have one phenyl ring which leans inwards and two which lean outwards, one of which has a very large canting angle of about 135°. However, the inwards phenyl ring of the anhydrous form is about 10° more closed than that of the hydrated form, while its outwards ring is about 10° more open than the corresponding ring in the hydrated form (Table 2). The cone conformation observed for the hydrated form is very close to the almost identical conformations observed for all seven independent molecules found in four solvate pseudo-polymorphs of hexahomotrioxacalix[3]arene functionalized with three phenylurea arms on the lower rim [43]. In the anhydrous form, the different conformation of the cone is accompanied by a two-position disorder of all three pyridyl arms (0.5/0.5, 0.5/0.5, and 0.7/0.3). In

the hydrated form, the two pyridyl groups attached to the outwards orientated phenyl rings are in an edge-to-face orientation, involving a CH···π interaction, while the pyridyl group attached to the inwards orientated phenyl ring is more external. This more external group and the pyridyl which is the face of the π interaction are involved as acceptors of H-bonds with water molecules, as is the O-atom of their interconnecting CH_2–O–CH_2 bridge. In fact, all the hydrogen atoms of the co-crystallized water and methanol atoms are involved in H-bonds, either with each other or with **PyHO3C3** molecules. This creates a 2D H-bond network and an interesting SOF with interconnected open channels filled with the co-crystallized solvent molecules (Figure 6). These channels account for more than 15% of the crystal volume (Table S5).

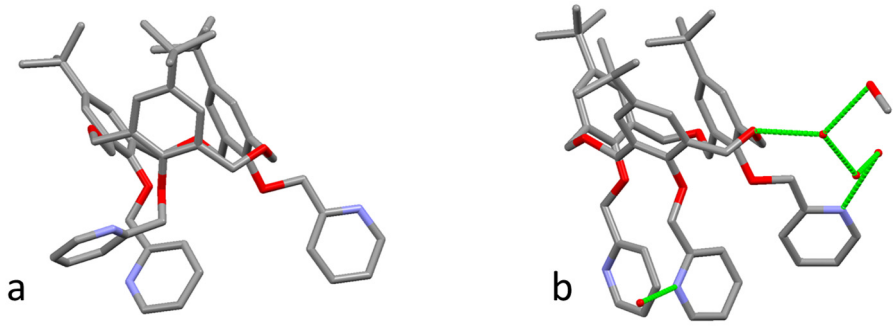

Figure 5. Asymmetric unit of two different **PyHO3C3** structures: (**a**) the anhydrous form **PyHO3C3** and (**b**) the hydrate form **PyHO3C3-H_2O-MeOH**. H-bonds between calixarene and co-crystallized solvent molecules are represented by green dashed lines. Hydrogen atoms have been omitted and only one position of the disorder groups is shown for better clarity. Atoms are in CPK colors.

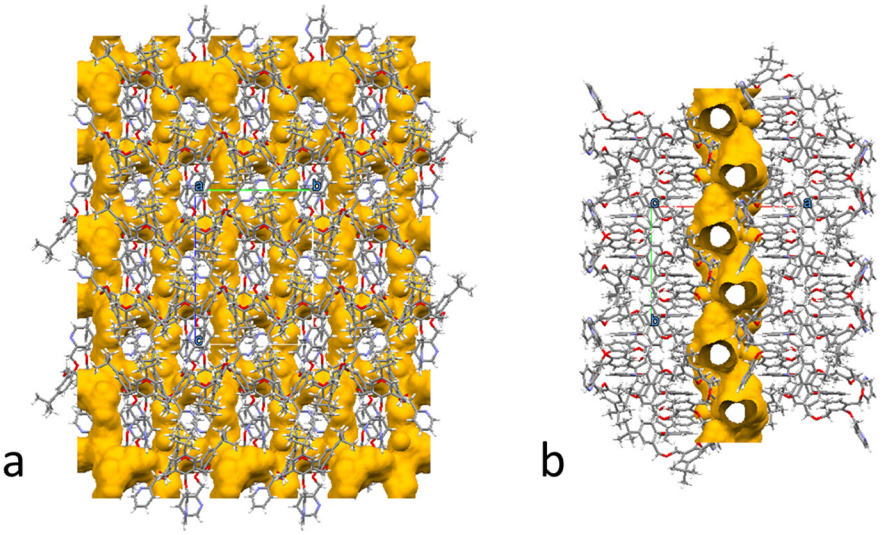

Figure 6. Crystal packing of **PyHO3C3-H_2O-MeOH** (**a**) viewed along the crystallographic *a* axis and (**b**) viewed along the crystallographic *a* axis. The surface of the solvent accessible volume calculated with a 1.2 Å probe evidences the 2D channel network developed in the (100) crystallographic plane. Atoms in CPK colors.

The examination of 11 crystal structures, with 15 crystallographically independent molecules, reveals that the conformation of the macrocycle is predominantly influenced by the presence of a guest molecule within the cavity, while the crystal packing and external solvent molecules play a limited role in shaping the solid-state cone conformation of these macrocycles. Despite the numerous crystallization attempts, the acetonitrile solvent forms host–guest complexes only with **PyC4** and **PyHOC4**, while this is not the case for **PyHO3C3,** indicating a lower affinity of this guest molecule for the most flexible

and less aromatic macrocycle, although the **PyHO3C3** cup and the acetronitrile molecule have the same C_3 symmetry. The observed closed conformation of **PyHO3C3**, along with the absence of the acetonitrile host–guest complex, can be rationalized in terms of a trade-off between competing dispersion interactions and entropic factors arising from the conformational freedom of **PyHO3C3** without a pre-formed cup. The acetonitrile guest molecule induces a notable conformational change, resulting in the opening of the cup in **PyC4** and **PyHOC4** (Figure 7). This alteration also affects the orientation of the 2-pyridylmethoxy arms attached on the lower rim of the macrocycles. The diverse conformations assumed by the 2-pyridylmethoxy groups involve face-to-face and edge-to-face orientations between the terminal aromatic rings.

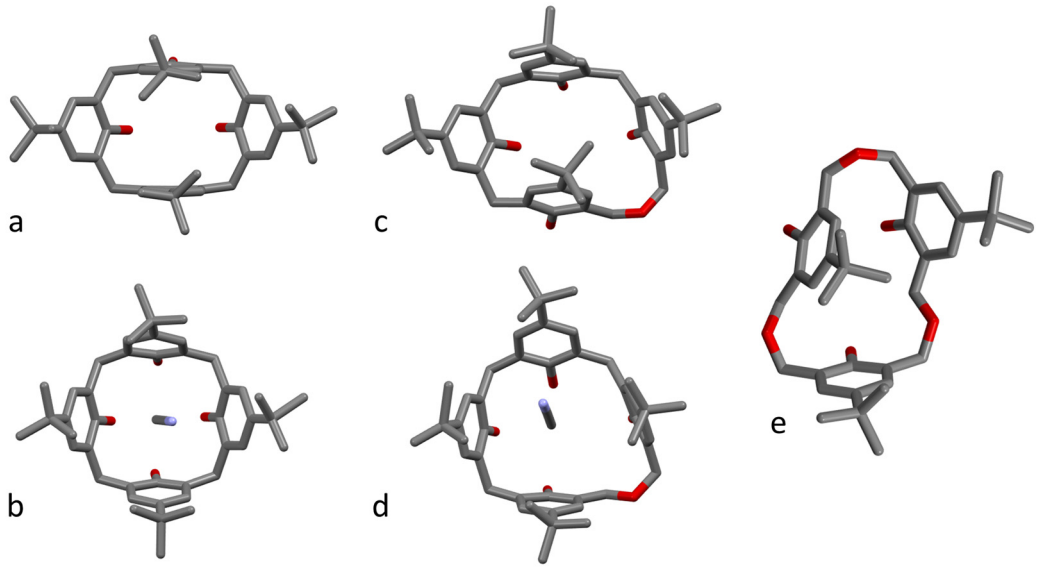

Figure 7. Effect of acetonitrile guest complexation on the macrocycle conformation. The cups are viewed perpendicular to the mean planes of the bridging methylene carbon atoms: (**a**) **PyC4**, (**b**) **PyC4⊂MeCN**, (**c**) **PyHOC4**, (**d**) **PyHOC4⊂MeCN**, (**e**) **PyHO3C3**. Atoms in CPK colors.

4. Conclusions

In conclusion, our investigation into the pseudo-polymorphism of 2-pyridylmethoxy cone derivatives of **PyC4**, **PyHOC4**, and **PyHO3C3** has provided valuable insights.

The 11 crystal structures reveal that the conformation of the macrocycle is predominantly influenced by the presence of an acetonitrile molecule which opens the cavity. Notably, only **PyC4** and **PyHOC4** produce a host–guest complex with acetonitrile, while the most flexible and less aromatic **PyHO3C3** does not give similar complexes.

While all the pseudo-polymorphs of **PyC4** exhibit a closely packed crystal structure (Table S5), **PyHOC4-hexane** and **PyHO3C3-H_2O-MeOH** present intriguing intertwined 1D and 2D solvent channel networks, respectively.

Notably, a correlation between the structural rigidity of the macrocycle and the number of pseudo-polymorphs formed has been observed. The more rigid macrocycle of **PyC4** displays a higher number (six) of pseudo-polymorphs, in contrast to the macrocycles with higher conformational flexibility, namely **PyHOC4** and **PyHO3C3**, which exhibit a minor number (three and two, respectively) of pseudo-polymorphs.

While caution is necessary in speculating about these findings due to the potential influence of specific crystallization conditions on polymorph formation, our results suggest a trend wherein more rigid molecules tend to form a diverse array of crystal packing. This observation adds depth to our understanding of the intricate relationship between molecular flexibility and the polymorphic behavior of calixarene derivatives.

This study not only underscores the complexity of crystal engineering in these systems, but also opens avenues for further exploration into the specific conditions governing the formation of different polymorphic forms.

Supplementary Materials: The following supporting information can be downloaded at: https://www.mdpi.com/article/10.3390/cryst14040343/s1. Figure S1: ORTEP drawing of the asymmetric unit for the **PyC4-MeOH-α** crystal form; Figure S2: ORTEP drawing of the asymmetric unit for the **PyC4-H2O-α** crystal form; Figure S3: ORTEP drawing of the asymmetric unit for the **PyC4-MeOH-β** crystal form; Figure S4: ORTEP drawing of the asymmetric unit for the **PyC4⊂MeCN-MeOH** crystal form; Figure S5: ORTEP drawing of the asymmetric unit for the **PyC4⊂MeCN-H_2O** crystal form; Figure S6: ORTEP drawing of the asymmetric unit for the **PyC4** crystal form; Figure S7: ORTEP drawing of the asymmetric unit for the **PyHOC4-DMSO** crystal form; Figure S8: ORTEP drawing of the asymmetric unit for the **PyHOC4⊂MeCN-MeOH** crystal form; Figure S9: ORTEP drawing of the asymmetric unit for the **PyHOC4-Hexane** crystal form; Figure S10: ORTEP drawing of the asymmetric unit for the **PyHO3C3** crystal form; Figure S11: ORTEP drawing of the asymmetric unit for the **PyHO3C3-H2O-MeOH** crystal form; Table S1: Summary of the various crystalline forms of **PyC4**, **PyHOC4**, and **PyH3OC3** obtained under various crystallization conditions. Table S2: Crystal data and structure refinements for **PyC4** pseudo-polymorphs; Table S3: Crystal data and structure refinements for **PyHOC4** pseudo-polymorphs; Table S4: Crystal data and structure refinements for **PyHO3C3** pseudo-polymorphs; Table S5: Total percentage solvent area volume per unit cell, including and excluding the co-crystallized solvent molecules.

Author Contributions: Conceptualization, S.G.; validation, S.J., N.H. and S.G.; investigation, S.J., N.H., P.M.M. and S.G.; writing—original draft preparation, S.J.; writing—review and editing, N.H, P.M.M. and S.G.; funding acquisition, S.G. All authors have read and agreed to the published version of the manuscript.

Funding: This work has received funding from MUR through the PRIN project 20227YNHEB.

Data Availability Statement: The X-ray crystallographic coordinates of the structures reported in this study were deposited at the Cambridge Crystallographic Data Centre (CCDC) under the deposition numbers CCDC 2331929-2331939. These data can be obtained free of charge from the CCDC at www.ccdc.cam.ac.uk/data_request/cif.

Acknowledgments: We thank the Elettra Synchrotron (Trieste, Italy) and the staff of the XRD1 beamline for their technical assistance.

Conflicts of Interest: The authors declare no conflict of interest.

References

1. Reinhoudt, D.N. Introduction and History. In *Calixarenes and Beyond*; Neri, P., Sessler, J.L., Wang, M.-X., Eds.; Springer International Publishing: Cham, Switzerland, 2016; pp. 1–11. ISBN 9783319318677.
2. Nimse, S.B.; Kim, T. Biological Applications of Functionalized Calixarenes. *Chem. Soc. Rev.* **2013**, *42*, 366–386. [CrossRef] [PubMed]
3. Kumar, R.; Sharma, A.; Singh, H.; Suating, P.; Kim, H.S.; Sunwoo, K.; Shim, I.; Gibb, B.C.; Kim, J.S. Revisiting Fluorescent Calixarenes: From Molecular Sensors to Smart Materials. *Chem. Rev.* **2019**, *119*, 9657–9721. [CrossRef] [PubMed]
4. Arora, V.; Chawla, H.M.; Singh, S.P. Calixarenes as Sensor Materials for Recognition and Separation of Metal Ions. *Arkivoc* **2007**, *2007*, 172–200. [CrossRef]
5. Pan, Y.C.; Hu, X.Y.; Guo, D.S. Biomedical Applications of Calixarenes: State of the Art and Perspectives. *Angew. Chem.-Int. Ed.* **2021**, *60*, 2768–2794. [CrossRef] [PubMed]
6. Giuliani, M.; Morbioli, I.; Sansone, F.; Casnati, A. Moulding Calixarenes for Biomacromolecule Targeting. *Chem. Commun.* **2015**, *51*, 14140–14159. [CrossRef] [PubMed]
7. Ludwig, R.; Dzung, N.T. Calixarene-Based Molecules for Cation Recognition. *Sensors* **2002**, *2*, 397–416. [CrossRef]
8. Español, E.S.; Villamil, M.M. Calixarenes: Generalities and Their Role in Improving the Solubility, Biocompatibility, Stability, Bioavailability, Detection, and Transport of Biomolecules. *Biomolecules* **2019**, *9*, 90. [CrossRef] [PubMed]
9. Naseer, M.M.; Ahmed, M.; Hameed, S. Functionalized Calix[4]arenes as Potential Therapeutic Agents. *Chem. Biol. Drug Des.* **2017**, *89*, 243–256. [CrossRef] [PubMed]
10. Böhmer, V. Calixarenes, Macrocycles with (Almost) Unlimited Possibilities. *Angew. Chem. Int. Ed. Engl.* **1995**, *34*, 713–745. [CrossRef]

11. Eddaif, L.; Shaban, A.; Telegdi, J. Sensitive Detection of Heavy Metals Ions Based on the Calixarene Derivatives-Modified Piezoelectric Resonators: A Review. *Int. J. Environ. Anal. Chem.* **2019**, *99*, 824–853. [CrossRef]
12. Quaglio, D.; Polli, F.; Del Plato, C.; Cianfoni, G.; Tortora, C.; Mazzei, F.; Botta, B.; Calcaterra, A.; Ghirga, F. Calixarene: A Versatile Scaffold for the Development of Highly Sensitive Biosensors. *Supramol. Chem.* **2021**, *33*, 345–369. [CrossRef]
13. Ren, H.; Wang, H.; Wen, W.; Li, S.; Li, N.; Huo, F.; Yin, C. A Summary of Calixarene-Based Fluorescent Sensors Developed during the Past Five Years. *Chem. Commun.* **2023**, *59*, 13790–13799. [CrossRef] [PubMed]
14. Sachdeva, G.; Vaya, D.; Srivastava, C.M.; Kumar, A.; Rawat, V.; Singh, M.; Verma, M.; Rawat, P.; Rao, G.K. Calix[n]arenes and Its Derivatives as Organocatalysts. *Coord. Chem. Rev.* **2022**, *472*, 214791. [CrossRef]
15. Zhou, J.; Yu, G.; Huang, F. Supramolecular Chemotherapy Based on Host–Guest Molecular Recognition: A Novel Strategy in the Battle against Cancer with a Bright Future. *Chem. Soc. Rev.* **2017**, *46*, 7021–7053. [CrossRef] [PubMed]
16. Patra, S.; Boricha, V.P.; Paul, P. Dual-Mode Calixarene-Based Chemosensor: Highly Selective Fluorogenic Detection of Hg^{2+} and Chromogenic Detection of Cu^{2+} with a Single Ionophore. *Eur. J. Inorg. Chem.* **2019**, *2019*, 199–205. [CrossRef]
17. Hussain, A.M.; Ashraf, U.M.; Muhammad, G.; Tahir, N.M.; Bukhari, N.A.S. Calixarene: A Versatile Material for Drug Design and Applications. *Curr. Pharm. Des.* **2017**, *23*, 2377–2388. [CrossRef] [PubMed]
18. Sliwa, W.; Girek, T. Calixarene Complexes with Metal Ions. *J. Incl. Phenom. Macrocycl. Chem.* **2010**, *66*, 15–41. [CrossRef]
19. Homden, D.M.; Redshaw, C. The Use of Calixarenes in Metal-Based Catalysis. *Chem. Rev.* **2008**, *108*, 5086–5130. [CrossRef] [PubMed]
20. Creaven, B.S.; Donlon, D.F.; McGinley, J. Coordination Chemistry of Calix[4]arene Derivatives with Lower Rim Functionalisation and Their Applications. *Coord. Chem. Rev.* **2009**, *253*, 893–962. [CrossRef]
21. Jin Mei, C.; Ainliah Alang Ahmad, S. A Review on the Determination Heavy Metals Ions Using Calixarene-Based Electrochemical Sensors. *Arab. J. Chem.* **2021**, *14*, 103303. [CrossRef]
22. Wilson, L.R.B.; Coletta, M.; Evangelisiti, M.; Piligkos, S.; Dalgarno, S.J.; Brechin, E.K. The Coordination Chemistry of P-Tert-Butylcalix[4]arene with Paramagnetic Transition and Lanthanide Metal Ions: An Edinburgh Perspective. *Dalt. Trans.* **2022**, *51*, 4213–4226. [CrossRef] [PubMed]
23. Pappalardo, S.; Giunta, L.; Foti, M.; Ferguson, G.; Gallagher, J.F.; Kaitner, B. Functionalization of Calix[4]arenes by Alkylation with 2-(Chloromethyl)Pyridine Hydrochloride. *J. Org. Chem.* **1992**, *57*, 2611–2624. [CrossRef]
24. Danil de Namor, A.F.; Castellano, E.E.; Pulcha Salazar, L.E.; Piro, O.E.; Jafou, O. Thermodynamics of Cation (Alkali-Metal) Complexation by 5,11,17,23-Tetra-Tert-Butyl[25,26,27,28-Tetrakis(2-Pyridylmethyl)Oxy]-Calix(4)arene and the Crystal Structure–Superstructure of Its 1:1 Complex with Sodium and Acetonitrile. *Phys. Chem. Chem. Phys.* **1999**, *1*, 285–293. [CrossRef]
25. Danil de Namor, A.F.; Piro, O.E.; Pulcha Salazar, L.E.; Aguilar-Cornejo, A.F.; Al-Rawi, N.; Castellano, E.E.; Sueros Velarde, F.J. Solution Thermodynamics of Geometrical Isomers of Pyridino Calix(4)arenes and Their Interaction with the Silver Cation. The X-Ray Structure of a 1:1 Complex of Silver Perchlorate and Acetonitrile with 5,11,17,23-Tetra-Tert-Butyl-[25,26,27,28-Tetrakis(2-Pyridylmethyl)oxy]- Calix(4)arene and the Crystal Structure–Superstructure of Its 1:1 Complex with Sodium and Acetonitrile. *J. Chem. Soc. Faraday Trans.* **1998**, *94*, 3097–3104. [CrossRef]
26. Marcos, P.M.; Teixeira, F.A.; Segurado, M.A.P.; Ascenso, J.R.; Bernardino, R.J.; Cragg, P.J.; Michel, S.; Hubscher-Bruder, V.; Arnaud-Neu, F. Complexation and DFT Studies of Lanthanide Ions by (2-Pyridylmethoxy)Homooxacalixarene Derivatives. *Supramol. Chem.* **2013**, *25*, 522–532. [CrossRef]
27. Neri, P.; Sessler, J.L.; Wang, M.-X. (Eds.) *Calixarenes and Beyond*; Springer Cham: New York, NY, USA, 2016; ISBN 978-3319318653.
28. Yamato, T.; Haraguchi, M.; Nishikawa, J.I.; Ide, S.; Tsuzuki, H. Synthesis, Conformational Studies, and Inclusion Properties of Tris[(2-Pyridylmethyl)Oxy]Hexahomotrioxacalix[3]arenes. *Can. J. Chem.* **1998**, *76*, 989–996. [CrossRef]
29. Xie, H.-F.; Wu, C.; Zou, J.; Yang, Y.-X.; Xu, H.; Zhang, Q.-L.; Redshaw, C.; Yamato, T. A Pyrenyl-Appended C3v-Symmetric Hexahomotrioxacalix[3]arene for Selective Fluorescence Sensing of Iodide. *Dye Pigment.* **2020**, *178*, 108340. [CrossRef]
30. Gutsche, C.D.; Bauer, L.J. Calixarenes. 13. The Conformational Properties of Calix[4]arenes, Calix[6]arenes, Calix[8]arenes, and Oxacalixarenes. *J. Am. Chem. Soc.* **1985**, *107*, 6052–6059. [CrossRef]
31. Augusto, A.S.; Miranda, A.S.; Ascenso, J.R.; Miranda, M.Q.; Félix, V.; Brancatelli, G.; Hickey, N.; Geremia, S.; Marcos, P.M. Anion Recognition by Partial Cone Dihomooxacalix[4]arene-Based Receptors Bearing Urea Groups: Remarkable Affinity for Benzoate Ion. *Eur. J. Org. Chem.* **2018**, 5657–5667. [CrossRef]
32. Araki, K.; Hashimoto, N.; Otsuka, H.; Shinkai, S. Synthesis and Ion Selectivity of Conformers Derived from Hexahomotrioxacalix[3]arene. *J. Org. Chem.* **1993**, *58*, 5958–5963. [CrossRef]
33. Fischer, C.; Gruber, T.; Eissmann, D.; Seichter, W.; Weber, E. Unusual Behavior of a Calix[4]arene Featuring the Coexistence of Basic Cone and 1,2-Alternate Conformations in a Solvated Crystal. *Cryst. Growth Des.* **2011**, *11*, 1989–1994. [CrossRef]
34. Taylor, D.; Ling, I.; Vilela, F.; Dalgarno, S.J. Intermolecular Interactions Drive the Unusual Co-Crystallization of Different Calix[4]arene Conformations. *Crystals* **2022**, *12*, 250. [CrossRef]
35. Marcos, P.M.; Ascenso, J.R.; Pereira, J.L.C. Synthesis and NMR Conformational Studies of *p-tert*-Butyldihomooxacalix[4]arene Derivatives Bearing Pyridyl Pendant Groups at the Lower Rim. *Eur. J. Org. Chem.* **2002**, 3034–3041. [CrossRef]
36. Cragg, P.J.; Drew, M.G.B.; Steed, J.W. Conformational Preferences of O-Substituted Oxacalix[3]arenes. *Supramol. Chem.* **1999**, *11*, 5–15. [CrossRef]
37. Kabsch, W. XDS. *Acta Crystallogr. Sect. D Biol. Crystallogr.* **2010**, *66*, 125–132. [CrossRef] [PubMed]

38. Kabsch, W. Integration, Scaling, Space-Group Assignment and Post-Refinement. *Acta Crystallogr. Sect. D Biol. Crystallogr.* **2010**, *66*, 133–144. [CrossRef] [PubMed]
39. Sheldrick, G.M. SHELXT—Integrated Space-Group and Crystal-Structure Determination. *Acta Crystallogr. Sect. A Found. Crystallogr.* **2015**, *71*, 3–8. [CrossRef] [PubMed]
40. Sheldrick, G.M. Crystal Structure Refinement with SHELXL. *Acta Crystallogr. Sect. C* **2015**, *71*, 3–8. [CrossRef]
41. Hickey, N.; Iuliano, V.; Talotta, C.; De Rosa, M.; Soriente, A.; Gaeta, C.; Neri, P.; Geremia, S. Solvent and Guest-Driven Supramolecular Organic Frameworks Based on a Calix[4]arene-Tetrol: Channels vs. Molecular Cavities. *Cryst. Growth Des.* **2021**, *21*, 6357–6363. [CrossRef]
42. Miranda, A.S.; Marcos, P.M.; Ascenso, J.R.; Berberan-Santos, M.N.; Schurhammer, R.; Hickey, N.; Geremia, S. Dihomooxacalix[4]arene-Based Fluorescent Receptors for Anion and Organic Ion Pair Recognition. *Molecules* **2020**, *25*, 4708. [CrossRef]
43. Teixeira, F.A.; Ascenso, J.R.; Cragg, P.J.; Hickey, N.; Geremia, S.; Marcos, P.M. Recognition of Anions, Monoamine Neurotransmitter and Trace Amine Hydrochlorides by Ureido-Hexahomotrioxacalix[3]arene Ditopic Receptors. *Eur. J. Org. Chem.* **2020**, *2020*, 1930–1940. [CrossRef]